arXiv:cond-mat/0610092v1 [cond-mat.mtrl-sci] 4 Oct 2006

Phase diagram of Pb(Zr,Ti)O_3 solid solutions from first principles

Igor A. Kornev[1], L. Bellaiche[1], P.-E. Janolin[2], B. Dkhil[2], and E. Suard[3]

[1]*Physics Department, University of Arkansas, Fayetteville, Arkansas 72701, USA*

[2] *Laboratoire Structures, Propriétés et Modélisation des Solides,*
Ecole Centrale Paris, CNRS-UMR8580,
Grande Voie des Vignes, 92295 Châtenay-Malabry Cedex, France

[3] *Institut Laue-Langevin, 6 rue Jules Horowitz,*
BP 156 38042, Grenoble Cedex, France

(Dated: February 6, 2008)

Abstract

A first-principles-derived scheme, that incorporates ferroelectric and antiferrodistortive degrees of freedom, is developed to study finite-temperature properties of $\mathrm{Pb(Zr_{1-x}Ti_x)O_3}$ solid solutions near its morphotropic phase boundary. The use of this numerical technique (i) resolves controversies about the monoclinic ground-state for some Ti compositions, (ii) leads to the discovery of an overlooked phase, and (iii) yields three multiphase points, that are each associated with four phases. Additional neutron diffraction measurements strongly support some of these predictions.

The ferroelectric $\mathrm{Pb(Zr_{1-x}Ti_x)O_3}$ (PZT) system is an example of perovskite solid solutions that are of high technological relevance because of their widespread use in piezoelectric transducers and actuators [1]. Its phase diagram in a narrow compositional region centered around x=0.50, and denoted as the morphotropic phase boundary (MPB) [2], also makes PZT of large fundamental importance. For instance, recent measurements have discovered an unexpected ferroelectric (FE) monoclinic phase [3] - that leads to high electromechanical coefficients [4, 5] and acts as a structural bridge between the well-known FE tetragonal and rhombohedral phases [3, 5]. Moreoever, another overlooked monoclinic phase has been recently observed [6, 7, 8, 9], in which the usually-competing [10] ferroelectric distortions and antiferrodistortive (AFD) motions (that are associated with the oxygen octahedra rotation) *coexist*. However, many controversies still surround this latter monoclinic phase, such as its exact space group, the axis about which the oxygen octahedra rotate and even if it is a minority phase rather than the long-range ground-state [6, 7, 8, 9].

In view of these findings, one may also wonder if *other* surprises – such as other overlooked phase(s) or multiphase points (that are unusual thermodynamic features [11]) – can still be in store for PZT. Some features could indeed have been missed because of (i) the difficulties in growing and characterizing at various temperatures many samples with tiny compositional differences; and (ii) the current lack of theoretical tools that are able to accurately compute finite-temperature properties of perovskite alloys. For instance, the two sole first-principles-based finite-temperature schemes [5, 12] that yield a monoclinic phase in the phase diagram of disordered PZT have some shortcomings: the alloy effective Hamiltonian model of Ref. [5] gives Curie temperatures that are $\simeq 60\%$ larger than measurements and does not include AFD motions, while we are not aware of any study reporting the accuracy of the bond-valence model of Ref. [12] for transition temperatures in PZT.

The purpose of this Letter are three-folds: (1) to demonstrate that it is possible to develop a numerical scheme able to accurately compute finite-temperature properties of perovskite solid solutions and that incorporates both FE and AFD motions; (2) to apply such scheme to resolve the controversies discussed above, as well as, to reveal some striking overlooked effects in the MPB of PZT; and (3) to experimentally confirm some of these discoveries, via neutron diffractions.

Our numerical scheme is based on the generalization of the first-principles-derived alloy effective Hamiltonian of Ref. [5] to include AFD effects, in addition to FE degrees of freedom.

The total energy is thus written as a *sum* of two main terms, $E_{\mathrm{FE}}(\{\mathbf{u}_i\},\{\eta_H\},\{\eta_I\},\{\sigma_j\})$ and $E_{\mathrm{AFD-C}}(\{\mathbf{u}_i\},\{\eta_H\},\{\eta_I\},\{\sigma_j\},\{\omega_i\})$, where E_{FE} is the energy provided in Ref. [5], while $E_{\mathrm{AFD-C}}$ is an additional term gathering AFD motions and their couplings in solid solutions. $\mathbf{u}_i$ is the local soft mode (which is directly proportional to the dipole) in unit cell i; $\{\eta_H\}$ and $\{\eta_I\}$ are the homogeneous and inhomogeneous strain tensors [13], respectively; σ_j=+1 or -1 corresponds to the presence of a Zr or Ti atom, respectively, at the B-lattice site j of the $\mathrm{Pb(Zr_{1-x}Ti_x)O_3}$ system. Finally, $\{\omega_i\}$ is a (B-centered) vector characterizing the direction and magnitude of the AFD motions in unit cell i. For instance, $\omega_i = 0.1\mathbf{z}$ corresponds to a rotation of the oxygen octahedra by 0.1 radians about the z-axis. For $E_{\mathrm{AFD-C}}$, we propose the following expression that contains five major terms:

$$\begin{aligned} E_{\mathrm{AFD-C}}(\{\mathbf{u}_i\},\{\eta_H\},\{\eta_I\},\{\sigma_j\},\{\omega_i\}) = \sum_i [\kappa_A\omega_i^2 + \alpha_A\omega_i^4 + \gamma_A(\omega_{i,x}^2\omega_{i,y}^2 + \omega_{i,y}^2\omega_{i,z}^2 + \omega_{i,x}^2\omega_{i,z}^2)] \\ + \sum_{i,j}\sum_{\alpha,\beta} K_{ij,\alpha\beta}\,\omega_{i,\alpha}\omega_{j,\beta} + \sum_i\sum_{\alpha,\beta} C_{l,\alpha\beta}\,\eta_l(i)\,\omega_{i,\alpha}\omega_{i,\beta} \\ + \sum_i\sum_{\alpha,\beta,\gamma,\delta} D_{\alpha\beta\gamma\delta}\,\omega_{i,\alpha}\omega_{i,\beta}u_{i,\gamma}u_{i,\delta} + \sum_i \omega_i[A_0\sigma_i + \sum_j A_1\sigma_j] \end{aligned} \tag{1}$$

where the sums over i run over all B-sites while the sums over j run over the six B nearest neighbors of the B-site i. $\eta_l(i)$ is the l^{th} component, in Voigt notation, of the total strain (i.e., homogeneous and inhomogeneous parts) at the site i. α, β, γ and δ denote Cartesian components, with the x-, y- and z-axes being along the pseudo-cubic [100], [010] and [001] directions, respectively. The first four terms of Eq. (1) characterize energertics of the hypothetical *simple* $\mathrm{Pb}{<}\,B\,{>}\mathrm{O_3}$ system resulting from the use of the virtual crystal approximation (VCA) [14] (via averaging of the Zr and Ti potentials) to mimic $\mathrm{Pb(Zr_{0.5}Ti_{0.5})O_3}$, while the last term represents how the actual atomic distribution affects the AFD motions. The first four terms are the self-energy associated with AFD motions, the short-range interaction energy between AFD degrees of freedom, the interaction energy between strain and ω_i, and the interaction energy between local-modes and AFD motions, respectively. The κ_A, α_A and γ_A parameters, as well as the $K_{ij,\alpha\beta}$, $C_{l,\alpha\beta}$ and $D_{\alpha\beta\gamma\delta}$ matrices (that greatly simplify due to symmetry), are determined by performing local-density-approximation (LDA) calculations [14, 15] on 10 atom-supercells of $\mathrm{Pb}{<}\,B\,{>}\mathrm{O_3}$. On the other hand, the A_0 and A_1 parameters are evaluated from LDA calculations on supercells containing *real* Zr and Ti atoms in addition to VCA atoms. Note that the proposed expression for $E_{\mathrm{AFD-C}}$ differs from the one of Ref. [10] for simple perovskites by its analytical expressions and the incorporation of alloying effects.

The total energy of our effective Hamiltonian is used in Monte-Carlo (MC) simulations to compute finite-temperature properties of PZT systems. We use $12 \times 12 \times 12$ supercells (8640 atoms) and up to 4 million MC sweeps, as well as decrease the temperature in small steps, to get well-converged results. The $\{\sigma_j\}$ variables are chosen randomly to mimic disordered alloys. Outputs of the MC procedure identify the space group of the predicted phases, and are: the homogeneous strain tensor $\{\eta_H\}$, the $< \mathbf{u} >$ supercell average of the local mode vectors $\{\mathbf{u}_i\}$, and the $< \omega >_R$ vector defined as $< \omega >_R = \frac{1}{N} \sum_i \omega_i (-1)^{n_x(i)+n_y(i)+n_z(i)}$, where the sum runs over the N sites i and where $n_x(i)$, $n_y(i)$ and $n_z(i)$ are integers locating the cell i (i.e., the B-site i is centered at $[n_x(i)\mathbf{x} + n_y(i)\mathbf{y} + n_z(i)\mathbf{z}]a$, where a is the lattice constant of PZT and where $\mathbf{x}$, $\mathbf{y}$ and $\mathbf{z}$ are unit vectors along the Cartesian axes). A non-vanishing $< \mathbf{u} >$ indicates ferroelectricity while a non-zero $< \omega >_R$ characterizes AFD motions associated with the R-point of the cubic first Brillouin zone. We also use the correlation functions of Refs [16] to precisely determine transition temperatures.

Figure 1(a) shows the x-, y- and z-Cartesian coordinates ($< u_1 >$, $< u_2 >$ and $< u_3 >$) of $< \mathbf{u} >$ in disordered $\mathrm{Pb(Zr_{0.52}Ti_{0.48})O_3}$ as a function of temperature, as predicted by the alloy effective Hamiltonian approach of Ref. [5] *that does not include AFD effects.* Figures 1(b) and 1(c) display $< \mathbf{u} >$ and $< \omega >_R$, respectively, in the same material, but when using the present method – with $< \omega_1 >_R$, $< \omega_2 >_R$ and $< \omega_3 >_R$ denoting the x-, y- and z-Cartesian coordinates of $< \omega >_R$. Figure 1(a) indicates that neglecting AFD motions and its couplings with ferroelectricity and strain leads to (1) a transition from a cubic paraelectric $Pm\bar{3}m$ phase (in which $< \mathbf{u} >$ is close to zero) to a tetragonal $P4mm$ ferroelectric phase (in which $< u_3 >$ drastically increases while $< u_1 >$ and $< u_2 >$ remain nearly null) around 825K ± 5K – which is higher than the experimental Curie temperature of $\simeq 663 \pm 5$ K [17] ; and (2) a tetragonal-to-monoclinic Cm transition, for which $< u_1 >$ and $< u_2 >$ now increase and become equal to each other while still being smaller in magnitude than $< u_3 >$, at 250K ± 13K. Comparing Figs 1(b-c) with Fig 1(a) reveals that turning *on* AFD motions has dramatic effects on the phase transition sequence – as correctly guessed by Ref. [18]. As a matter of fact, two new phases – with both FE and AFD components – are found at the lowest temperatures, namely monoclinic Cc between $\simeq$ 163 K and $\simeq$ 138 K and rhombohedral $R3c$ below 138 K ± 6 K. Furthermore, the theoretical

Curie temperature is decreased down to 413 K ± 13 K, which now makes it smaller than the measurement [17]. This discrepancy is due to the fact that the effective Hamiltonian parameters were determined at the (underestimating) theoretical LDA lattice constant. As a matter of fact, we numerically found that the pressure leading to our theoretical volume matching the experimental one [6] at low temperature is -4.68 GPa, and that the use of this negative pressure within the present numerical scheme results in the $< \mathbf{u} >$ and $< \omega >_R$ displayed in Figs 1(d) and (e), respectively. The resulting theoretical Curie temperature is now $\simeq 650 \pm 13\,\mathrm{K}$, which is in excellent agreement with the measured value of $\simeq 663 \pm 5$ K. Moreover, the symmetry of the purely FE phases coincides with those measured at this specific composition [6], that is tetragonal $P4mm$ and monoclinic Cm when decreasing the temperature. Our simulations also predict the existence of a monoclinic state below $138\,\mathrm{K} \pm 13\,\mathrm{K}$ in which ferroelectricity cohabits with AFD motions, as consistent with the electron-diffraction reflections observed in Ref. [6] below 150 K. Furthermore, we confirm the findings of Refs [6, 7, 8] that the correct space group for the low-temperature phase of $\mathrm{Pb(Zr_{0.52}Ti_{0.48})O_3}$ is Cc rather than Pc, as initially proposed in Ref. [9]. Moreover, this Cc phase is indeed the (long-range-ordered) ground-state of $\mathrm{Pb(Zr_{0.52}Ti_{0.48})O_3}$ rather than a minority phase coexisting with the purely FE Cm phase for the lowest temperatures, as suggested in Ref. [6]. Finally, the oxygen octahedra in this Cc phase do *neither* rotate about the [001] direction (as thought in Ref. [9]) nor about the [111] direction (as proposed in Ref. [6]) but rather about an axis that is in-between the [001] and [111] directions (which is in agreement with Ref. [8]), since Fig 1(e) shows that, at the smallest temperatures, $< \omega_3 >_R$ is larger in magnitude than $< \omega_1 >_R$ and $< \omega_1 >_R = < \omega_2 >_R$. Interestingly, this axis of rotation does *not* precisely coincide with the direction of the polarization - since the “FE” ratio $\frac{<u_3>}{<u_2>}$ differs from the “AFD” ratio $\frac{<\omega_3>_R}{<\omega_2>_R}$ – which contrasts with the assumption of Ref. [8].

We now turn our attention to Fig. 2 that displays the phase diagram of $\mathrm{Pb(Zr_{1-x}Ti_x)O_3}$ near the MPB, as predicted by the present scheme with a -4.68 GPa pressure. Seven phases exist within a narrow compositional range. Five of such phases are well-known, namely paraelectric $Pm\bar{3}m$, FE rhombohedral $R3m$, FE tetragonal $P4mm$, FE monoclinic Cm, and the rhombohedral $R3c$ state in which ferroelectricity coexists with AFD motions. The sixth phase is the previously “controversial” Cc phase discussed above, and that is the ground-state at intermediate Ti compositions. (Note that the monoclinic phases are predicted to exist for the narrow Ti compositional range of 46.3 %–51.5%, which agrees remarkably well with the experimental range of $\simeq$ 46%-52% [17, 19].) The last phase occurs at small temperature and for the largest displayed Ti compositions, and has never been suggested to be a possible ground-state of PZT (to the best of our knowledge). This phase has a $I4cm$ space group, also involves a coexistence of ferroelectricity and rotation of oxygen octahedra, but is associated with the *tetragonal* symmetry (unlike $R3c$ and Cc). As a result, an increase in Ti concentration from $\simeq$ 47% to 52% results not only in a spontaneous polarization continuously rotating from [111] to [001] but also to the oxygen octahedra varying their rotation axis from [111] to [001] – via the [uuv] directions in the bridging monoclinic structures Cm and Cc phases. [We also checked that *no* AFD state associated with an off-center k-point *different* from R exists in the MPB of PZT.] Other features of Fig. 2 going against common beliefs [6, 8] are the *non-verticality* of the temperature-composition boundary lines separating rhombohedral from monoclinic structures. As a result, *five* different phases emerge for some narrow compositions. For instance, for x $\simeq$ 47.2%, our scheme predicts the $Pm\bar{3}m$, $P4mm$, Cm, $R3m$ and $R3c$ phases when decreasing the temperature. Similarly, a Ti concentration around 47.5% yields a $Pm\bar{3}m$ – $P4mm$ – Cm – Cc – $R3c$ sequence [20]. Finally, Fig. 2 further reveals the existence of three temperature-compositional points, for which *four* phases are very close to each other! (Multiphase points are unusual thermodynamic features [11].) The first multiphase point gathers the paraelectric $Pm\bar{3}m$ state and the FE $R3m$, Cm and $P4mm$ phases, and occurs for $T \simeq 610\,\mathrm{K}$ and $x \simeq 46.3$ % [21]. (Note that a quadruple point in which the paraelectric state coexists with three FE phases was also predicted to exist in the phase diagrams of epitaxial PZT thin films [22].) Two purely FE phases meet with two phases exhibiting a coexistence of FE and AFD motions for the other two multiphase points. More precisely, $R3m$, Cm, $R3c$ and Cc all meet at $T \simeq 150$ K and $x \simeq 47.4\%$, while Cm, $P4mm$, Cc and $I4cm$ overlap at T $\simeq$ 100 K and x $\simeq$ 0.495.

We have also undertaken a Rietveld analysis of neutron data on a $\mathrm{Pb(Zr_{0.49}Ti_{0.51})O_3}$ sample, collected at 10K at the ILL thermal source on the powder diffractometer D2B (λ=1.6 Å). Analysis of the data collection from 2Θ=20 to 140 degrees with a 2Θ step of 0.05 degrees was carried out with the XND software [23], using pseudo-Voigt peak-shape function including asymmetric broadening and linear interpolation for the background. The fluctuation in the sample's composition was estimated to be $\simeq$ 0.003 based on x-ray peaks at 300K and dielectric measurement. We observed superlattice reflections in the diffraction pattern (not shown here), and thus considered different space groups that are associated with doubled unit cells – namely, rhombohedral $R3c$, monoclinic Pc, Cc and Ic, and tetragonal $I4cm$. Each *single*-phase model leads to a considerable mismatch between the observed and calculated profiles for the pseudocubic reflections, and thus to poor agreement factors. A considerable improvement is achieved by considering *two*-phase coexistence models between the above space groups and also by including the monoclinic Cm and cubic $Pm\bar{3}m$ phases. The best agreement factors and matching between the observed and calculated profiles is obtained with the $I4cm$+Cc coexistence model (that results in R_{wp}, R_B and G.o.F. factors being equal to 6.69%, 5.09% and 1.72, respectively). Our structural refinement thus confirms the existence of the "controversial" Cc state (for which our structural parameters are very close to the ones of Ref. [24]) and of the presently-discovered $I4cm$ structure (for which the a, b and c parameters are equal to 5.700(2), 5.700(2) and 8.329(6) Å, respectively). Note that the proportion of $I4cm$ and Cc phases is approximately 7:3. The coexistence of these two phases may be due to compositional fluctuation in the sample, which will make this coexistence consistent with the theoretical phase diagram of Fig.2. It may also take its origin from the presence of small grains in the grown ceramic, since Ref. [25] predicts that the coexistence of different phases may be energetically favorable (over a single phase) in a ceramic of fixed composition when the grain size is small. We also hope that our other predictions, including the ones about multiphase points, will be experimentally confirmed soon.

This work is supported by ONR grants N00014-04-1-0413, N00014-01-1-0600 and N00014-01-1-0365, by NSF grants DMR-0404335, and by DOE grant DE-FG02-05ER46188. We thank B. Noheda for useful discussions.

---

[1] K. Uchino, (Kluwer Academic Publishers, Boston) (1996).

[2] M.E. Lines and A.M. Glass, *Principles and Applications of Ferroelectrics and Related Materials* (Clarendon Press, Oxford, 1977).

[3] B. Noheda, D.E. Cox, G. Shirane, J.A. Gonzalo, L.E. Cross, and S-E. Park, *Appl. Phys. Lett.* **74**, 2059 (1999).

[4] B. Noheda, D.E. Cox, G. Shirane, S.E. Park, L.E. Cross, and Z. Zhong, *Phys. Rev. Lett.*, **86**,

3891 (2001).

[5] L. Bellaiche, A. García and D. Vanderbilt, *Phys. Rev. Lett.* **84**, 5427 (2000); *Ferroelectrics* **266**, 41-56 (2002).

[6] B. Noheda, L. Wu, and Y. Zhu, *Phys. Rev. B* **66**, 060103(R) (2002).

[7] D.M. Hatch, H.T. Stokes, R. Ranjan, Ragini, S.K. Mishra, D. Pandey and B.J. Kennedy, *Phys. Rev. B* **65**, 212101 (2002).

[8] D.J. Woodward, J. Knudsen and I.M. Reaney, *Phys. Rev. B* **72**, 104110 (2005).

[9] R. Ranjan, Ragini, S.K. Mishra, D. Pandey and B.J. Kennedy, *Phys. Rev. B* **65**, 060102(R) (2002).

[10] D. Vanderbilt and W. Zhong, *Ferroelectrics* **206**, 181 (1998).

[11] M. L. Plumer, A. Caill and K. Hood *Phys. Rev. B* **39**, 4489 (1989).

[12] I. Grinberg, V.R. Cooper and A.M. Rappe *Nature* **419**, 909 (2002).

[13] W. Zhong, D. Vanderbilt and K.M. Rabe, *Phys. Rev. Lett.* **73**, 1861 (1994); *Phys. Rev. B* **52**, 6301 (1995).

[14] L. Bellaiche and D. Vanderbilt, *Phys. Rev. B* **61**, 7877 (2000).

[15] P. Hohenberg and W. Kohn, *Phys. Rev.* **136**, B864 (1964); W. Kohn and L.J. Sham, *ibid.* **140**, A1133 (1965).

[16] A. García and D. Vanderbilt, *Appl. Phys. Lett.* **72**, 2981 (1998); *First-Principles Calculations for Ferroelectrics: Fifth Williamsburg Workshop*, R.E. Cohen, ed. (AIP, Woodbury, New York, 1998), p. 53.

[17] B. Noheda, J.A. Gonzalo, L.E. Cross, R. Guo, S.-E. Park, D.E. Cox and G. Shirane, *Phys. Rev. B* **61**, 8687 (2000).

[18] M. Fornari and D.J. Singh, *Phys. Rev. B* **63**, 092101 (2001).

[19] K. C. Lima, A. G. Filho, A. P. Ayala, J. Mendes Filho, P. T. Freire, F. E. Melo, E. B. Arajo, and J. A. Eiras, *Phys. Rev. B* **63**, 184105 (2001).

[20] Ref. [6] indicates that the Ti composition, for which the $P4mm$-to-Cm transition occurs at 300K is $\simeq$ 48% while our scheme predicts that this happens for $x \simeq 47.3\%$. This slight disagreement may be due to the difficulty for the simulations to accurately reproduce the strong compositional dependency of the $P4mm$-to-Cm transition temperature (see Fig. 2), or that real samples have compositional inhomogeneities.

[21] The simulations in Fig. 2 provide Curie temperatures that are in very good agreement with

measurement for $x \simeq 48\%$, but that begin to underestimate (respectively, overestimate) experimental data by more than 50 K for x smaller than 46.5% (respectively, larger than 50.5%) [6]. As a result, the first multiphase point may be experimentally found at a temperature slightly larger than 610 K.

[22] N.A. Pertsev, V.G. Kukhar, H. Kohlstedt and R. Waser, *Phys. Rev. B* **67**, 054107 (2003).

[23] J.F. Bérar, *IUCr. Sat. Meeting on Powder Diffractometry*, Toulouse (1990).

[24] R. Ranjan, A.K. Singh, Ragini, and D. Pandey, *Phys. Rev. B* **71**, 092101 (2005).

[25] A.G. Zembilgotov, N.A. Pertsev and R. Waser, *J. Appl. Phys.* **97**, 114315 (2005).

FIG. 1: Supercell average $< \mathbf{u} >$ of the local mode vectors (Panels (a), (b) and (d)) and AFD-related $< \omega >_R$ quantity (Panels (c) and (e)), as a function of temperature in $\mathrm{Pb(Zr_{0.52}Ti_{0.48})O_3}$. Panel (a) corresponds to predictions from the use of the alloy effective Hamiltonian method of Refs. [5] – that neglects AFD effects. Panels (b) and (c) (respectively, Panels (d) and (e)) shows the results of the presently proposed method with no applied pressure (respectively, when applying a pressure of −4.68GPa).

FIG. 2: Phase diagram of $\mathrm{Pb(Zr_{1-x}Ti_x)O_3}$ near its MPB, as predicted by the present scheme with an applied pressure of −4.68GPa. Symbols display the direct results of our simulations, while lines are guide for the eyes. Indices 1, 2 and 3 indicate the multiphase points. The uncertainty on the transition temperatures is typically around 13 K, except close to the multiphase points 2 and 3 for which this uncertainty is around 3 K.

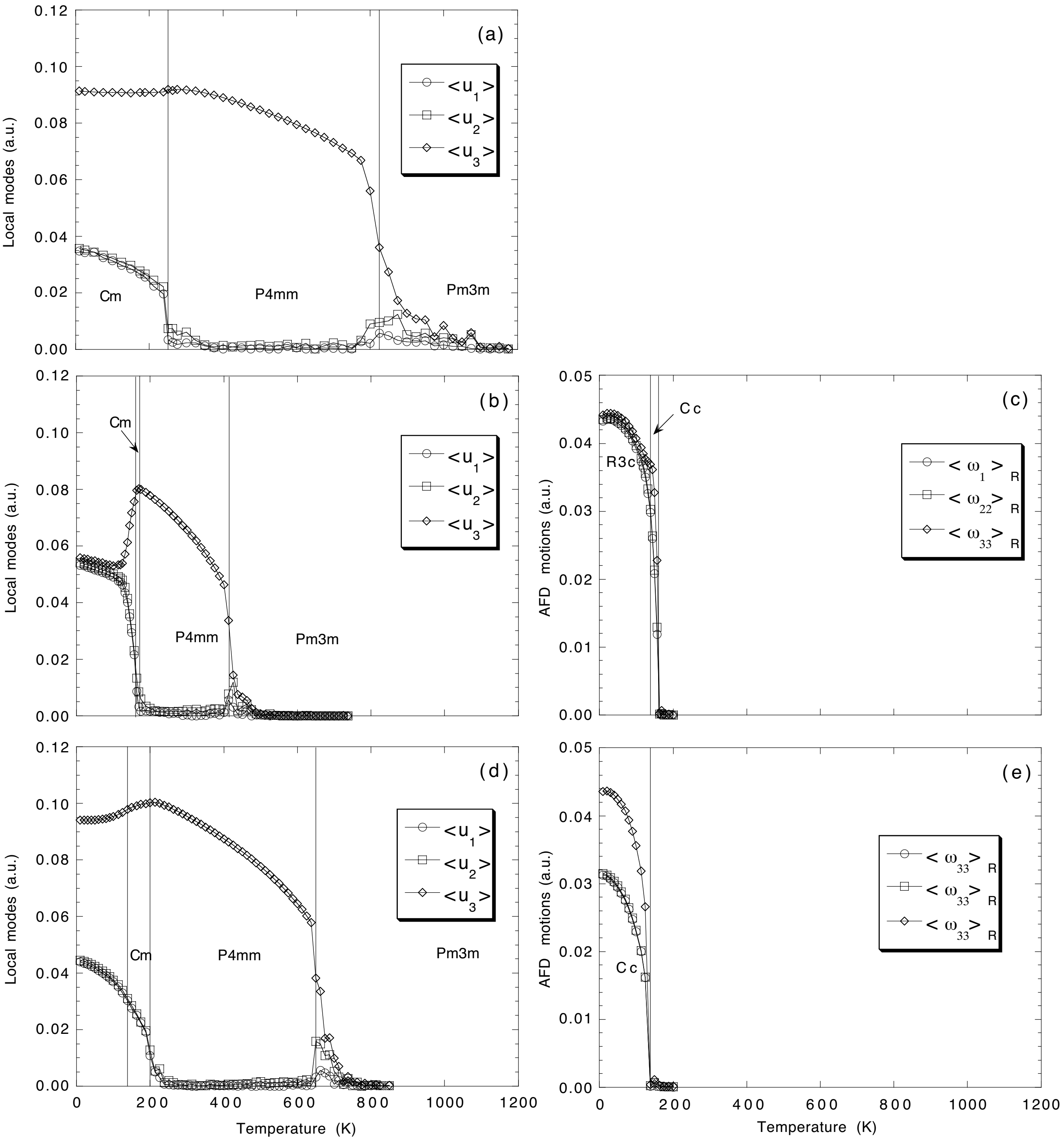
(a)
Local modes (a.u.)
0.12
0.10
0.08
0.06
0.04
0.02
0.00
<u1>
<u2>
<u3>
Cm
P4mm
Pm3m
(b)
Cm
P4mm
Pm3m
(c)
AFD motions (a.u.)
0.05
0.04
0.03
0.02
0.01
0.00
Cc
R3c
< ω1 >R
< ω22 >R
< ω33 >R
(d)
Cm
P4mm
Pm3m
0
200
400
600
800
1000
1200
Temperature (K)
(e)
< ω33 >R
< ω33 >R
< ω33 >R
Cc

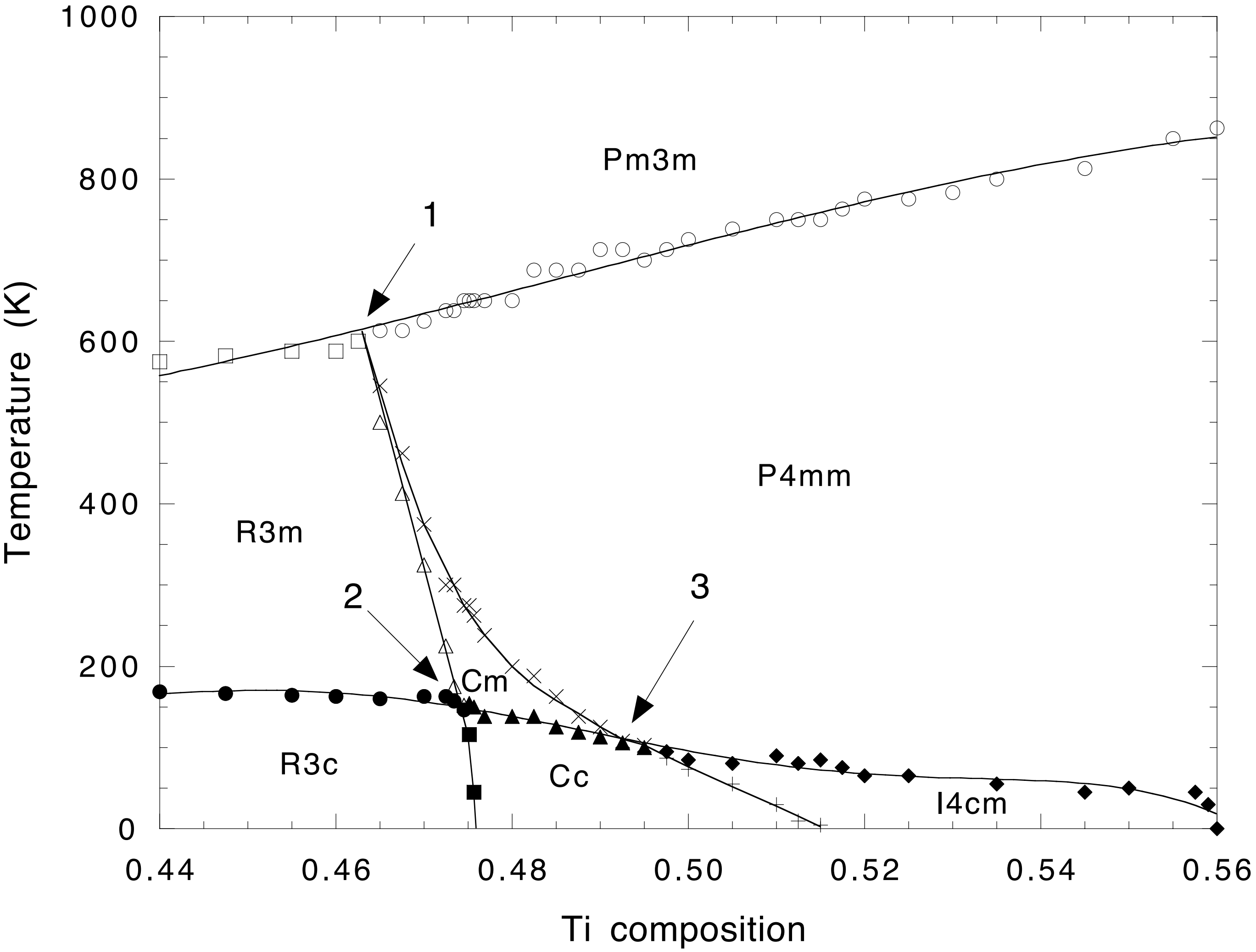
1000
800
600
400
200
0
Temperature (K)
0.44
0.46
0.48
0.50
0.52
0.54
0.56
Ti composition
Pm3m
P4mm
R3m
R3c
Cm
Cc
I4cm
1
2
3